Hindawi Publishing Corporation
Journal of Nanomaterials
Volume 2015, Article ID 609273, 12 pages
http://dx.doi.org/10.1155/2015/609273

Research Article

Nanoflake Manganese Oxide and Nickel-Manganese Oxide Synthesized by Electrodeposition for Electrochemical Capacitor

Man Van Tran,[1] An The Ha,[2] and Phung My Loan Le[1,2]

[1]*Department of Physical Chemistry, Faculty of Chemistry, University of Science, VNUHCM, 227 Nguyen Van Cu Street, District 5, Ho Chi Minh City 70000, Vietnam*
[2]*Applied Physical Chemistry Laboratory, Faculty of Chemistry, University of Science, VNUHCM, 227 Nguyen Van Cu Street, District 5, Ho Chi Minh City 70000, Vietnam*

Correspondence should be addressed to Phung My Loan Le; lmlphung@hcmus.edu.vn

Received 15 January 2015; Accepted 24 March 2015

Academic Editor: Jumi Yun

Nanoflake structures of electrochemical manganese oxide (EMD) and nickel mixed manganese oxide (NiMD) were directly deposited on a stainless steel by using Chronoamperometry and Cyclic Voltammetry (CV) techniques. The structure, morphology, and capacitive behavior of EMD or NIMD nanoflake were affected by the electrodeposition modes and deposition time. The highest specific capacitance (C_{sp}) was obtained for only two-minute deposition by both methods. EMD nanoflakes electrodeposited by CV technique show higher specific capacitance values than those prepared by Chronoamperometry owing to its homogenous and highly porous surface. All EMD samples exhibited excellent cycle behavior, less than 5% capacitance loss after 1000 cycles. Ni mixed MnO_2 was prepared at different Mn^{2+}/Ni^{2+} ratios for 2 minutes of electrodeposition. The presence of Ni^{2+} ion enhanced the C_{sp} value at high charge-discharge rate due to the decrease of the charge transfer resistance. The supercapacitor prototype of 2 cm × 2 cm was assembled using EMD and NiMD as electrode material and tested at 1 $A \cdot g^{-1}$.

1. Introduction

Nanomaterials such as nanowires, nanorods, nanotubes, and nanoparticles have attracted great interest due to their unique physical properties (electrical, optical, and magnetic) and catalyst and chemical properties [1, 2]. Mostly used materials for supercapacitors include carbon materials, conducting polymers, and transitions metal oxides [1]. Manganese oxide shows excellent pseudocapacitive behavior with the large specific capacitance over 700 F/g in spite of the theoretical value of 1100 F/g [1, 3, 4]. Manganese oxide is a promising electrode material in supercapacitor due to its low cost, natural abundance, and being environmentally friendly compared to other pseudocapacitor materials [3]. In recent years, nanostructured manganese oxides have been thoroughly investigated for different potential applications such as catalysis for synthetic organic chemistry, water treatment, and energy storage devices [1–3]. Nanostructured manganese oxide was synthesized by chemical methods and physical methods. However, chemical methods have more benefits due to simplicity, economical effectiveness, and ability to control various structures and morphologies. Several methods have been suggested like chemical reduction, hydrothermal, sonochemistry electrochemical deposition, and sol-gel method [3]. The structural parameters such as crystal form, defect chemistry, morphology, porosity, and texture play a crucial role in determining and optimizing the electrochemical properties when using MnO_2 as electrode materials (Table 1) [3].

One of the most common methods is electrochemical deposition due to its abilities to control the film thickness, structure, and morphology [5–9]. Pang et al. potentiostatically prepared the first electrodeposited thin film MnO_2 electrode for electrochemical capacitor (ECs) in 2000 and their finding had sparked strong interest among energy research community for its application in supercapacitor electrode [5, 6]. Such high specific capacitance value arises from the ions insertion/desertion within MnO_2 structure and it depends crucially on the particle size, surface, and porosity. Most of

Table 1: Synthesis method, physicochemical features, and subsequent specific capacitance of crystalline MnO_2.

Technique	Morphology	Structure	$S_{BET}/m^2 \cdot g^{-1}$	Capacitance C, F/g
Hydrothermal [17]	Platelike, nanorod	α-MnO_2	100–150	72–160 (200 mA·g^{-1})
High viscosity process [18]	Rod-shaped	α-MnO_2, γ-MnO_2	—	389 (10 mV·s^{-1})
Room temperature precipitation [19]	Rod-shaped	δ-MnO_2	—	201
Low temperature reduction [20]	Nanoflower	Cubic MnO_2 (Fd3m)	225.9	121.5 (1000 mA·g^{-1})
Sol-gel process [21]	Nanorods	γ-MnO_2		317 (100 mA·g^{-1})

following studies have focused on varying the deposition parameters in order to achieve the enhanced electrochemical performance [7–13]. The MnO_2 thin films can be prepared by anodic/cathodic electrodeposition. Cationic Mn^{2+} precursor is used in anodic oxidation while anionic MnO_4^- (Mn^{7+}) is used in cathodic reduction. In comparison, cathodic reduction offers more versatility as various metals could be codeposited during the deposition process. Oxidation of the metallic substrate during anodic deposition could also be avoided [14–16].

In this work, MnO_2 (EMD) and Ni mixed MnO_2 (NiMD) were electrochemically synthesized by Cyclic Voltammetry (CV) and Chronoamperometry (CA) and characterized for supercapacitor application. For Ni mixed MnO_2, the Ni content of binary oxide was investigated to find out the optimized capacitive value, high power density, and electrochemical stability. Material characterization was carried out by Transmission Electron Microscopy (TEM), Raman spectroscopy, Infrared Spectroscopy, Cyclic Voltammetry (CV), and charge-discharge cycling. Excellent capacitor values and stability of binary oxide Ni-MnO_2 were demonstrated.

2. Experimental

2.1. Synthesis Process. All chemical reagents are analytical grades: $MnSO_4 \cdot H_2O$ (99%, Sigma Aldrich), Na_2SO_4 (99%, Prolabo Chemical), and $Ni(NO_3)_2 \cdot 6H_2O$ (Sigma Aldrich). For MnO_2 electrochemical deposition, aqueous solutions of 0.3 M $MnSO_4$ and 0.05 M Na_2SO_4 (solution A) were prepared in distilled water just before use. The pH of solution A is neutral (pH ~ 7).

Stainless steel (SS) sheet of grade 214 with 2 cm × 2 cm surface and thickness of 0.5 mm was used as substrate for electrodeposition. The EMD and NiMD samples were performed by using Biologic-MPG 2 potentio/galvanostat system at room temperature in three-electrode cell. The electrochemical cell includes a stainless steel as working electrode (WE), a titanium mesh as auxiliary electrode (AE), and a saturated Ag/AgCl (in 3 M KCl) electrode as reference electrode (RE).

EMD and NiMD materials were synthesized by Chronoamperometry (CA) and Cyclic Voltammetry (CV) method. By using CA method, MnO_2 thin film was deposited in galvanostatic mode at 1.2 V versus Ag/AgCl on SS substrate. In CV method, MnO_2 thin film was formed during potential sweep in range of 0-1 V versus Ag/AgCl (sat) at scan rate of 50 mV/s. The deposition time of EMD samples was investigated from 2 to 12 minutes for each method (Table 2).

Table 2: Abbreviation of EMD samples prepared by two electrodeposition methods.

Time (minutes)	CV method	CA method
2	EMD-CV2	EMD-C2
4	EMD-CV4	EMD-C4
6	EMD-CV6	EMD-C6
8	EMD-CV8	EMD-C8
10	EMD-CV10	EMD-C10

2.2. Characterization. The structure of electrodeposited samples was characterized by using Raman spectroscopy and Fourier Transform Infrared Spectrometer (FTIR) IFS 28 Brucker. The IR absorption was carried out over the wavelength range 400–4000 cm^{-1}. The surface morphology and particle size were determined using a Scanning Electron Microscopy (SEM) JSM 6480 LV and Transmission Electron Microscopy (TEM) JEOL JEM 1400. Stylus Profilometer was carried out by Dektak 6 M equipment in order to determine thickness of MnO_2 films. The contact angle of thin film was measured using Data Physics Optical Contact Angle OCA20 in order to check the wetting property in aqueous solution.

The capacitive behavior of thin film electrodes was evaluated in 1 M Na_2SO_4 electrolyte. The electronic resistance of thin film as well as assembled supercapacitor prototype was studied by electrochemical impedance spectroscopy (EIS) in a frequency range of 10^{-5} to 10^{-2} Hz. The three-electrode cell consisted of thin film MnO_2 on SS as working electrode, platinum wire as auxiliary electrode, and electrode reference (Ag/AgCl for aqueous solution). The CV measurements were carried out at in 0-1 V versus Ag/AgCl (sat). The C_{sp} was calculated by using the following equation:

$$C_{sp} = \frac{Q}{m\Delta V}, \quad (1)$$

where Q: charge area calculated from integration of half CV curve, m: the mass of electrode material, and ΔV: the width of potential window.

The specific capacitance (C_{sp}) of supercapacitor was also evaluated by Galvanostatic charge-discharge method. The 2 × 2 cm supercapacitor prototypes, containing electrodeposited material on SS substrates used as current collector, were used for cycling test and were charged-discharged at current density of 1 A·g^{-1}.

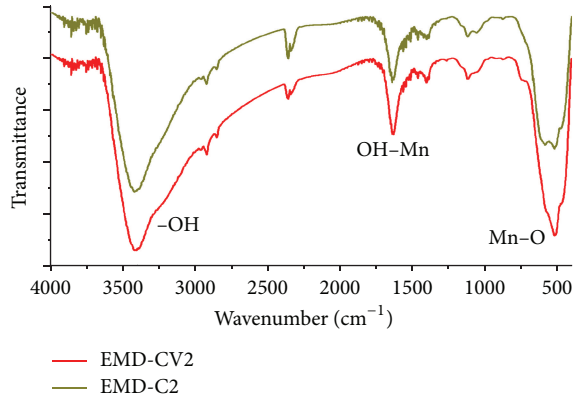

Figure 1: Infrared spectra of EMD-C2 and EMD-CV2.

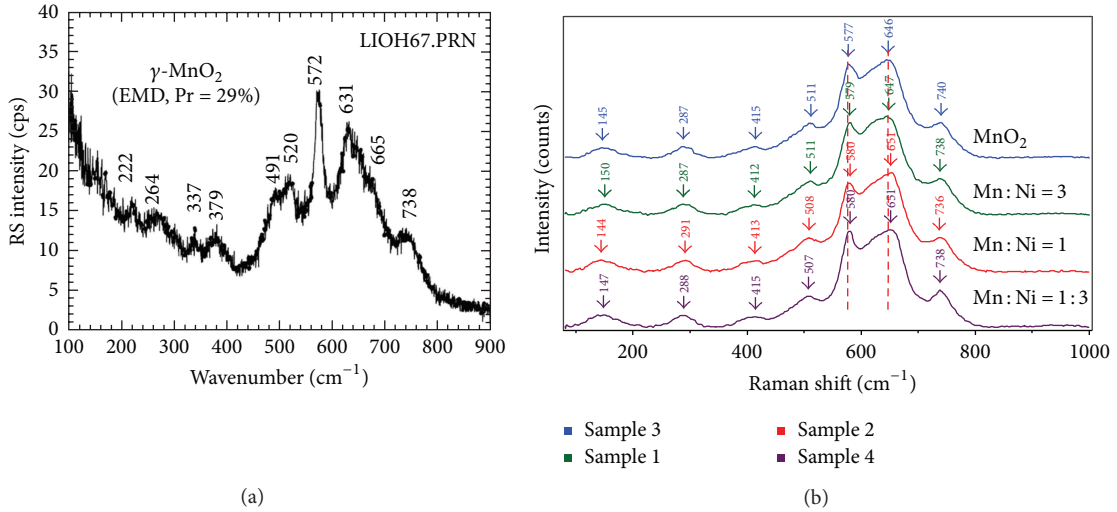

Figure 2: Raman spectra of electrodeposited MnO_2 (EMD-C2) and NiMD with different Mn^{2+} : Ni^{2+} ratios (3 : 1; 1 : 1; 1 : 3).

3. Results and Discussion

3.1. FTIR and Raman Characterization. The structure of thin films EMD and NiMD was characterized by using IR and Raman spectroscopy. Figure 1 showed the spectra of EMD deposited in 2 minutes by two methods in 400–4000 cm^{-1}. The samples were abbreviated as EMD-CV2 and EMD-C2.

The vibration at 3400 cm^{-1} indicated –OH vibration mode of the water. As thin film was prepared in the aqueous solution, a tunnel structure MnO_2 can be formed during the electrodeposited process. Thus, H_2O molecules can be intercalated in the tunnel of thin film [8]. The vibration bands at 1600 cm^{-1} and 500 cm^{-1} were assigned to Mn–O stretching modes of MnO_6 octahedral sites. These vibration modes are similar to those of natural mineral nsutite samples (γ-MnO_2 structure, complex tunnel), but some features are not clearly determined [8].

An examination of Raman spectroscopy is presented in Figure 2 for EMD and NiMD thin films with various Mn : Ni ratios. Compared to the study of Julien et al. [22], the vibration mode of MnO_2 thin film at 577 cm^{-1} (ν3), 640 cm^{-1} (ν2), and 740 cm^{-1} (ν1) corresponds to the stretching modes of the MnO_6 octahedral. The corresponding antisymmetry stretching modes are recorded in the infrared spectrum at 517 cm^{-1} and 621 cm^{-1} (Figure 2). The weak Raman bands at 511, 415, 297, and 145 cm^{-1} are assigned to the deformation modes of the metal-oxygen chain of Mn–O–Mn in the MnO_2 octahedral lattice. The Ni mixed MnO_2 (NiMD) sample exhibited similarly Raman vibration bands. However, the shifted modes were clearly observed, for example, the blue shift for (ν2) and (ν3) vibration and the red shift for (ν1) vibration. Also, the vibration peaks at lower wavenumber were shifted (Figure 2). The results showed that the presence of Ni ion affected the local structure of MnO_2, typically the short range environment of oxygen coordination around transition metal cations in MnO_2 lattice.

3.2. Morphology and Wettability Studies. Figures 3 and 4 show SEM images of EMD and NiMD thin films. The surface porosity and nanoflakes dimension were also affected by deposit time and the deposition mode. A slight difference was observed when the electrodeposition mode changed (Figures 3(a) and 3(c)). Generally, the surface morphology of thin films is composed entirely of nanoscale fiber (nanoflakes).

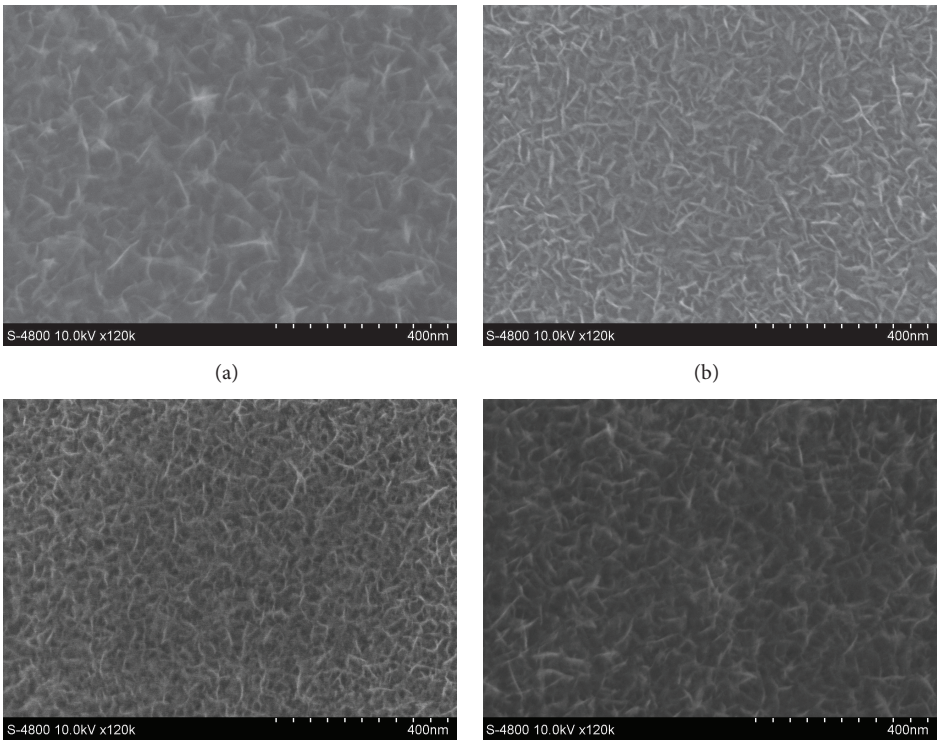

(a) (b)

(c) (d)

Figure 3: SEM images of EMD-C12 (a), EMD-CV2 (b), EMD-CV12 (c), and EMD-C2 (d).

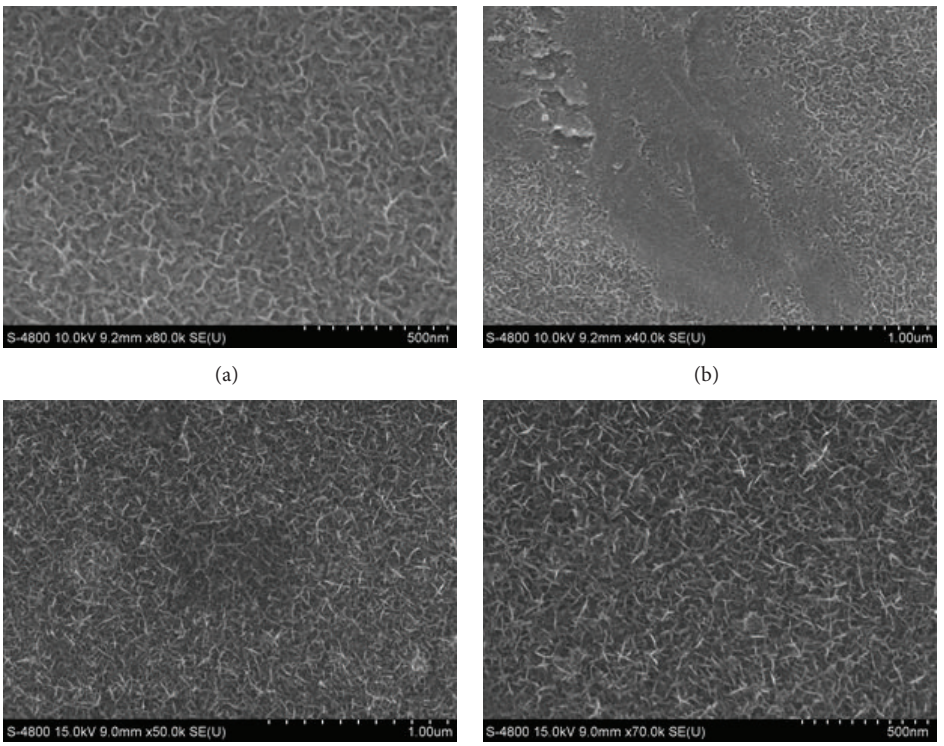

(a) (b)

(c) (d)

Figure 4: SEM images of NiMD prepared by CA (a, b) and by CV (c, d) in 2 minutes.

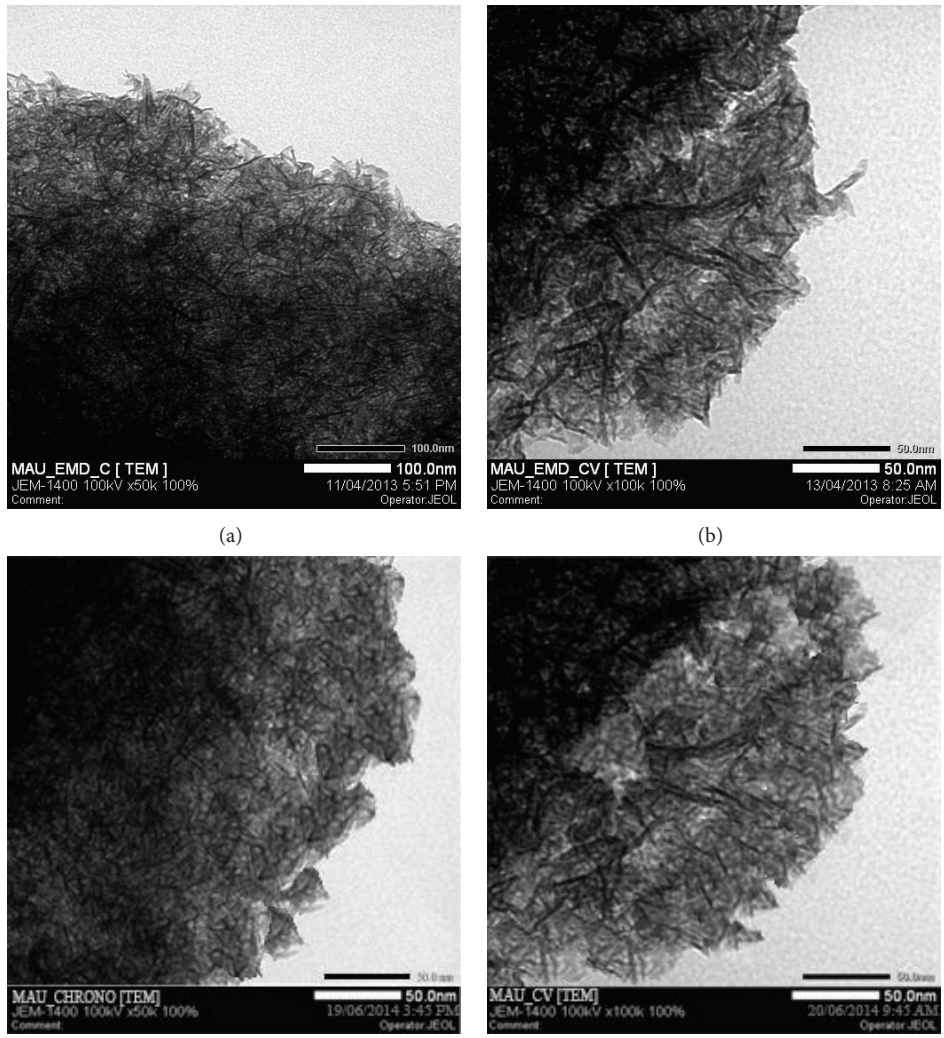

(a) (b)

(c) (d)

Figure 5: TEM images of EMD and NiMD prepared by CA method (a, c) and by CV method (b, d) in two minutes.

An irregular interconnection of nanofibers formed a highly porous network. By using CV method, the nanofiber slightly grows up. The nanoflakes dimension is about 100–120 nm in length compared to 40–60 nm of which prepared by CA method. As the deposition time is long, the nanofibers grow up quickly and the interconnection points seem to be a star form (Figures 3(c) and 3(d) for 12 minutes electrodeposition). Due to the variation of surface porosity and nanofiber morphology, the specific capacitance behavior is expectedly changed [1].

In case of Ni mixed MnO_2, the surface morphologies seem to be similar to those of MnO_2 films (Figure 4). Using CV method exhibits homogenous surface covered of well-formed nanoflakes.

TEM images were performed for Ni mixed MnO_2 (NiMD) at the same electrodeposition conditions (Figure 5). In general, it was observed that film structure prepared in two minutes is dense. The nanoflakes seem to be very fine and tend to interweave to make a network.

Wettability test is carried out in order to investigate the interaction between liquid and thin film surface. As the wettability is high, the small contact angle (θ) resulted and the surface is hydrophilic. In contrast, the surface is hydrophobic. Both hydrophilic and hydrophobic properties can be applied to many fields from medicine to engineering, especially in energy storages [1]. Figure 6 shows the contact angle measured for MnO_2 films prepared by CA and CV method. Both films are expectedly hydrophilic due to the presence of –OH group on the surface and in the structure. Indeed, the results in Figure 6 indicated that contact angle is less than 90°. In addition, EMD-CV2 thin film is more hydrophilic than EMD-C2. The hydrophilicity is essential for electrochemical reaction on the electrode/aqueous electrolyte interface.

3.3. Electrochemical Properties of Electrodeposited Thin Film. The capacitance behavior of MnO_2 and NiMD thin films was tested using CV in potential range of 0-1 V at 100 mV/s. Figure 7 shows CV curves of MnO_2 thin films prepared by CA and CV method in 1 M Na_2SO_4.

The specific capacitance (C_{sp}) was calculated by using (1). EMD was prepared by CA method; EMD-CA exhibited

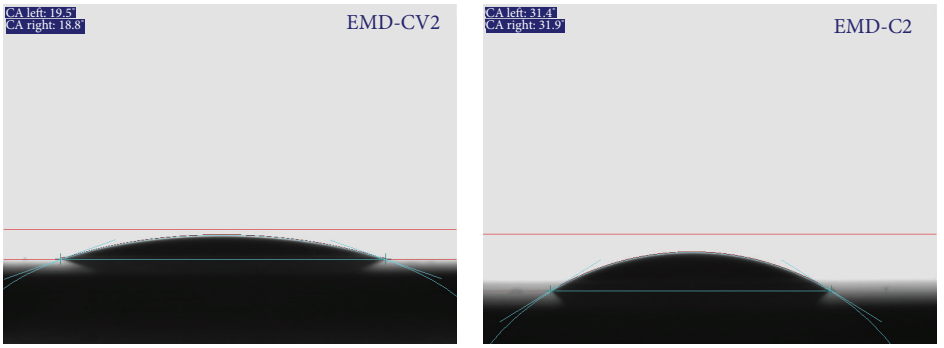

Figure 6: Water contact angle of EMD-CV2 (a) and EMD-C2 (b).

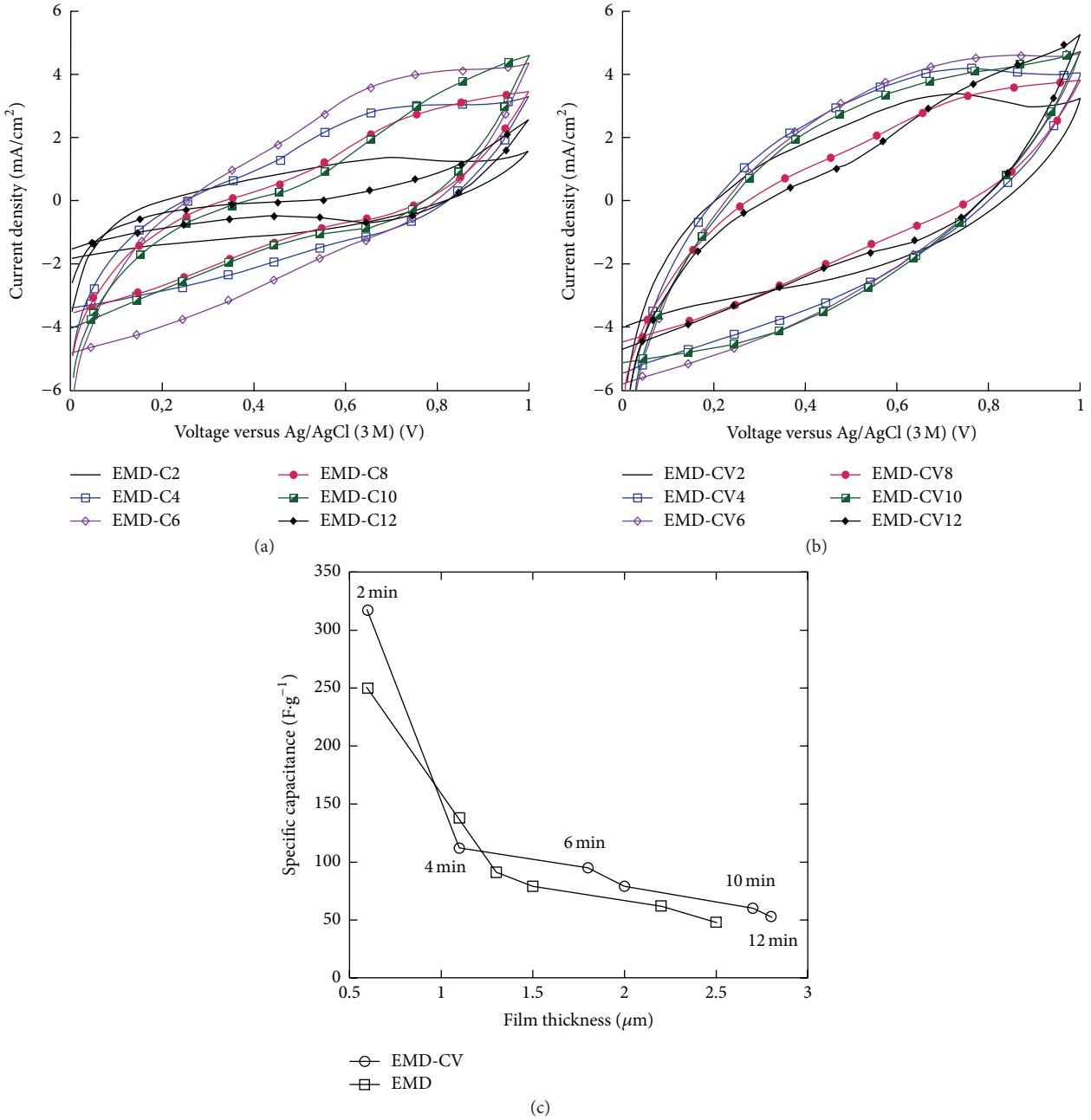

Figure 7: CV curves of EMD-C and EMD-CV samples in 2 M Na_2SO_4 at 100 mV/s (a, b). Plot of C_{sp} and thickness of EMD thin films corresponding to deposition time (c).

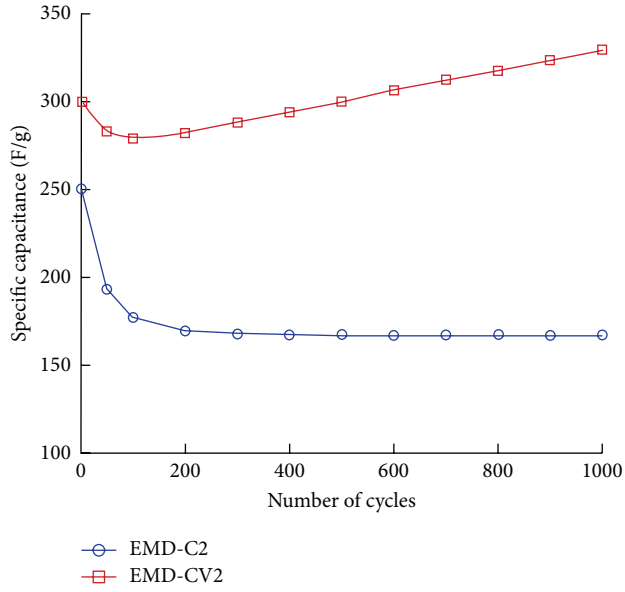

Figure 8: Electrochemical stability of EMD-C2 and EMD-CV2 at scan rate 100 mV/s.

the C_{sp} values that are 250, 138, 91, 79, 62, and 48 F/g for EMD-C2, EMD-C4, EMD-C6, EMD-C8, EMD-C10, and EMD-C12, respectively. With CV method, the C_{sp} values are 317, 112, 95, 79, 60, and 53 F/g for EMD-CV2, EMD-CV4, EMD-CV6, EMD-CV8, EMD-CV10, and EMD-CV12, respectively. Previous studies [2, 3, 6] show that capacitances of manganese oxide synthesized by electrochemical deposition were about 200–300 F/g.

The highest C_{sp} was obtained at two minutes of electrodeposition for both methods (Figure 7(c)). The thickness of MnO_2 film is about 0.55 μm. Thus, it can be concluded that the thin and porous film was only obtained in a short deposition time. When the deposition time is long, the nanoflakes grew up fast and their interconnection makes the film more compact than a short-time deposition. Thus, penetration of electrolyte into the film as well as the specific capacitance decreases due to the increase of electric resistance. The small thickness of MnO_2 film is necessarily required in order to obtain the good electric conductivity and specific capacitance [4, 12].

The electrochemical stability of thin films was evaluated. Figure 8 shows the specific capacitance (C_{sp}) of EMD-C2 and EMD-CV2 measured at a scan rate of 100 mV/s. Among EMD-C samples, the highest initial capacitance was obtained for EMD-C2. The C_{sp} value keeps constant, about 170 F/g after 200 cycles. For EMD-CV2, the C_{sp} decreases slightly after 100 cycles before increasing significantly to 330 F/g in the following cycles. After 1000 cycles, the fading of C_{sp} of EMD-C2 and EMD-CV2 was 23% and 5%, respectively (see Figure 10). Thus, the nanostructured EMD-CV2 seems to be better for supercapacitor application than EMD-C2. In fact, this fade observed for EMD samples can be explained by the structure evolution in aqueous solution, so the metal ion doping into MnO_2 lattice would improve the structural stability.

The two minutes electrodeposition was chosen to study the Ni mixed MnO_2 (NiMD) at different $Mn^{2+}:Ni^{2+}$ ratios. Figures 9(a) and 9(b) show the CV electrochemical properties of NiMD samples prepared by two deposition methods. In comparison to the EMD samples, the NiMD exhibited the same shape type of voltammogram but larger magnitude current. It can be observed that the CVs are more rectangular and symmetrical but lower in current magnitude at high Mn^{2+}/Ni^{2+} ratio than at the low ratio. Thus, the characteristics indicate the ideal capacitive behavior with high reversibility of NiMD sample. The highest C_{sp} was obtained for NiMD samples at $Mn^{2+}/Ni^{2+} = 1:1$ at all scan rates (Figures 9(c) and 9(d)).

The electrochemical stability of NiMD thin films prepared at $Mn^{2+}/Ni^{2+} = 1:1$ was also evaluated (Figure 11). In comparison to the EMD at the same deposition condition, NiMD samples exhibited higher C_{sp}, about 500 F/g versus 300 F/g. By changing the electrodeposition modes, the NiMD-CV shows the C_{sp} increase after 500 cycles, from 430 F/g to 500 F/g while NiMD-CA keeps constant during 800 cycles; after that a slight fading is observed at the final cycles. After 1000 cycles at 100 mV/s, the fading of C_{sp} is less than 7% for NiMD samples. The fact that Ni ion doping into MnO_2 lattice increases C_{sp} as well as electrochemical stability was briefly reported by Rajendra Prasad and Miura [23]. In this work, the highest C_{sp} was obtained about 480 F/g at 100 mV/s for NiMD sample (65% wt MnO_2 : 35% wt NiO).

3.4. Electrochemical Properties of Supercapacitor Prototype. Electrochemical impedance spectroscopy (EIS) measurements were also carried out in the frequency range of 100 kHz–0.1 Hz. Figure 11 shows the Nyquist plots of EMD thin films prepared at various deposition times by two methods.

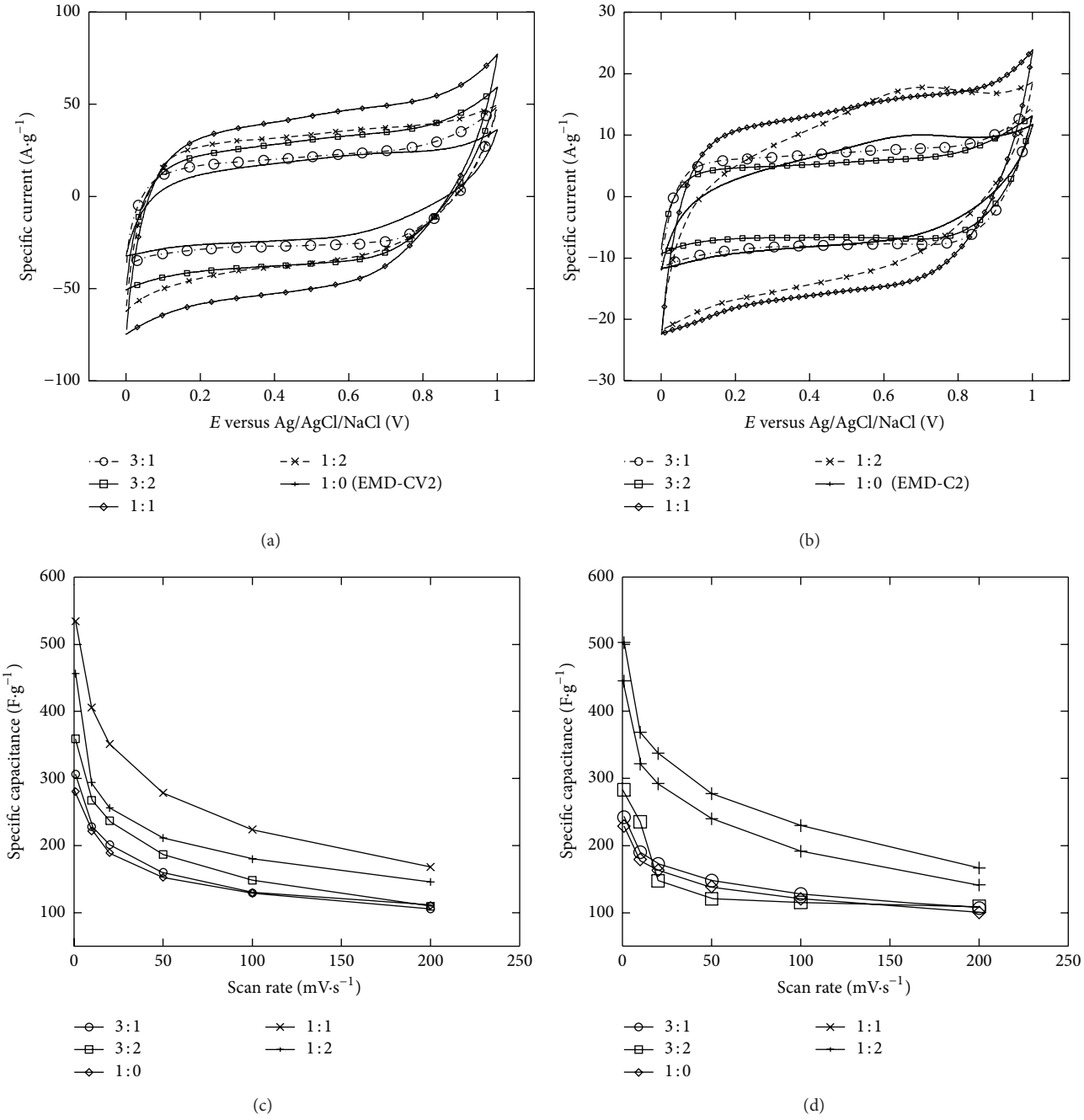

FIGURE 9: CV curves of Ni mixed MnO_2 (NiMD samples) prepared by CV method (a) and CA method (b) in 2 M Na_2SO_4 at 50 mV/s. Plot of C_{sp} as a function of scan rate (c, d).

The Nyquist plot shows a high-frequency intercept on the real axis corresponding to the electrolyte resistance (R_Ω); a semicircle is considered as a parallel combination of charge transfer resistance (R_{ct}) and double-layer capacitance (C_{dl}) with a linear region at low-frequency range. In the low-frequency region, linear part of the plot exhibits an angle between 45 and 90°.

The EIS data was analyzed by the electrical equivalent circuit which consists of (R_Ω) the electrolyte resistance, (R_{ct}) charge transfer resistance, constant phase element (CPE) used instead of double-layer capacitance (C_{dl}), Warburg (W) arising from a diffusion controlled process at low-frequency, and CPE assigned to pseudocapacitance of the material in the low-frequency because of nonideal capacitive behavior. The starting nonzero intercept at Z′ at beginning of semicircle is identical in all the curves and its electrical resistance of Na_2SO_4 around 1 Ω. For CA method, the charge transfer values of EMD-C2, EMD-C6, EMD-C8, and EMD-C12 are 43 Ω, 102 Ω, 116 Ω, and 126 Ω, respectively. For CV method, the charge transfer values of EMD-CV2, EMD-CV4,

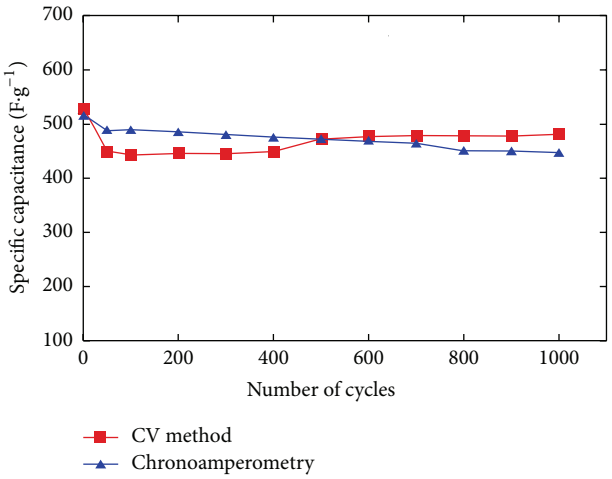

FIGURE 10: Electrochemical stability of NiMD samples prepared at $Mn^{2+}/Ni^{2+} = 1:1$ by two methods at scan rate 100 mV/s.

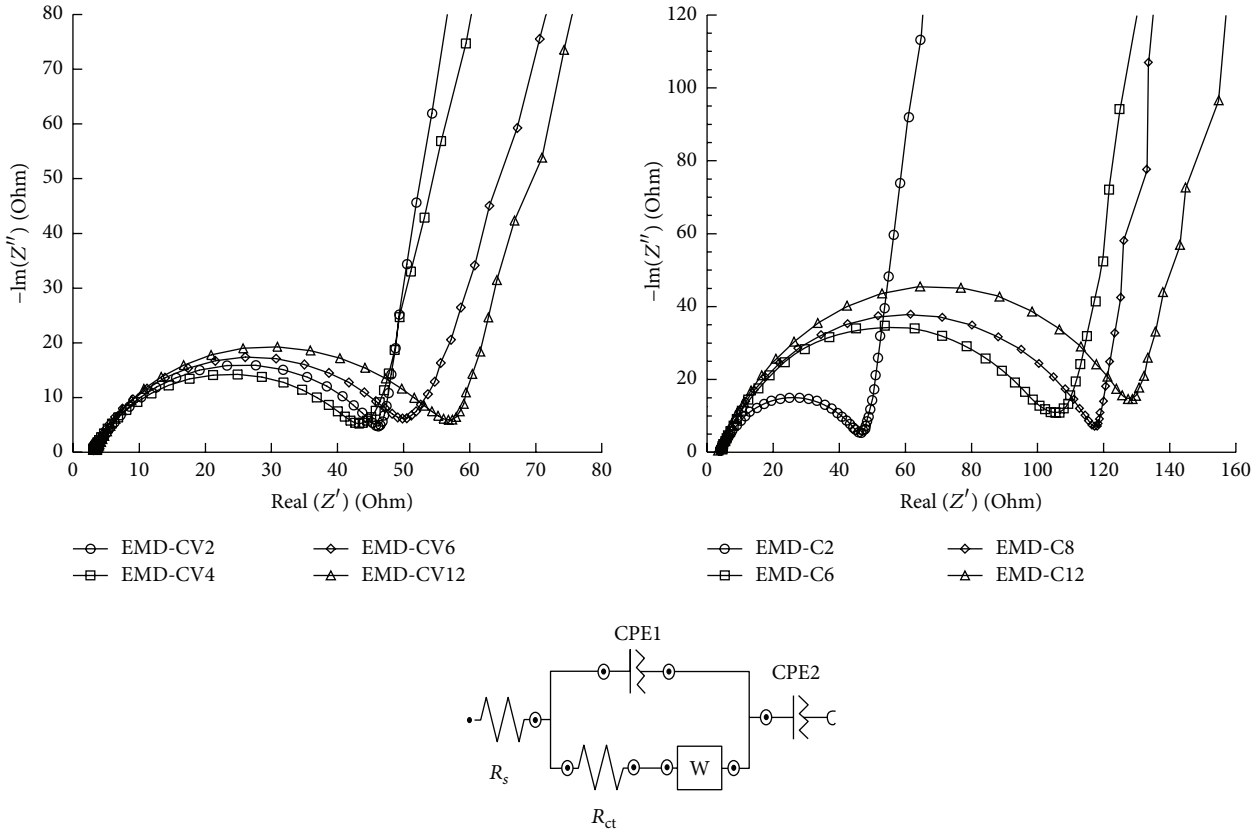

FIGURE 11: Nyquist plot of EMD thin films prepared by two methods and equivalent circuit model used for data fitting.

EMD-CV8, and EMD-CV12 are 40 Ω, 42 Ω, 47 Ω, and 55 Ω, respectively. It means that the increase of deposition time (or film thickness) decreases the charge transfer resistance. Thus, a high resistance caused a difficult charge transfer electron between interface electrolyte and interface electrode.

At the same deposition conditions, the charge transfer resistance of NiMD samples decreases significantly compared to EMD (Figure 12).

As the Mn^{2+}/Ni^{2+} increase, the semicircle diameter becomes smaller. The lowest resistance was obtained for NiIMD at $Mn^{2+}/Ni^{2+} = 1:1$, about 4 Ω versus 10 Ω at $Mn^{2+}/Ni^{2+} = 1:2$ (Figure 13).

The Ni ion addition to the MnO_2 lattice would improve the electrical resistivity of MnO_2 film in addition to enhance the specific capacitance. It maybe also enhanced the power density as well as reversibility of the supercapacitior at

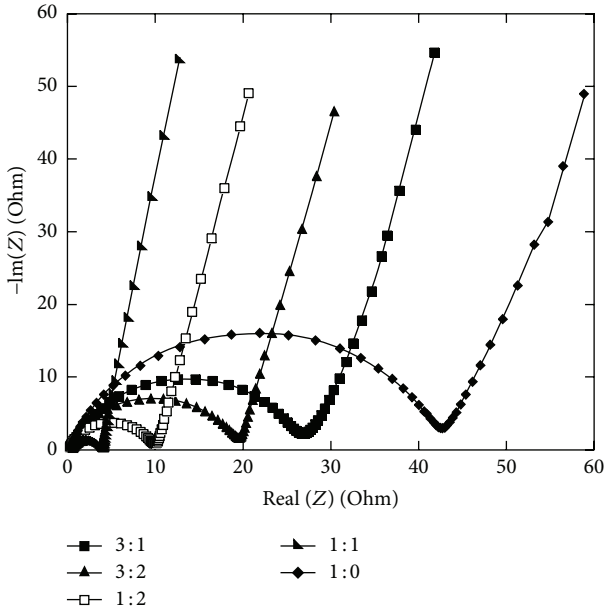

Figure 12: Nyquist plot of NiMD samples prepared by CA method compared to EMD-C2.

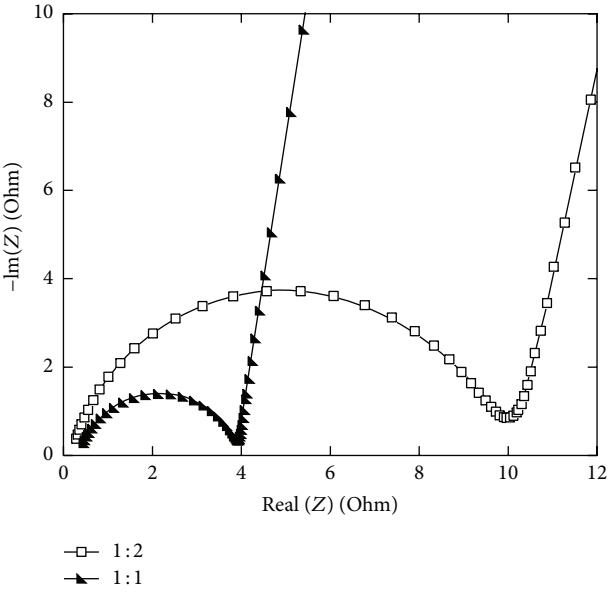

Figure 13: Nyquist plot (zoom part) of NiMD samples at $Mn^{2+} : Ni^{2+} = 1:1$ and 1 : 2.

high charge-discharge rate. Symmetrical capacitor prototypes of 2 cm × 2 cm were assembled with two thin films of electrodes EMD-CV2 and NiMD-CV at $Mn^{2+}/Ni^{2+} = 1:1$ and characterized by charge-discharge cycling at very high current $1\,A{\cdot}g^{-1}$.

Figure 14 shows charge-discharge values of EMD and NIMD sample at current $1\,A{\cdot}g^{-1}$. The efficiency of charge-discharge cycling is about 0.9. Discharge C_{sp} values were calculated by using the current density, discharge time, and the weight of material. C_{sp} values obtained from Figure 14 for EMD-CV2 and NiMD-CV are $10\,F{\cdot}g^{-1}$ and $25\,F{\cdot}g^{-1}$. As expected, supercapacitor of NiMD-CV based electrode exhibits a higher power density than EMD-CV2.

The stability of supercapacitor based on NiMD-CV and EMD-CV2 was also tested for a large number of cycles (up to 10,000 cycles) at $2\,A{\cdot}g^{-1}$. A C_{sp} fading of 25% and 14% was observed with NiMD-CV or EMD-CV2 based capacitors, respectively, after 10,000 charge-discharge cycles. There is an initial large C_{sp} decrease and then the C_{sp} remained almost constant. The NiMD-CV exhibited expectedly higher stability than EMD-CV2 based capacitor. Thus, it would be promising for the long-term capacitor application.

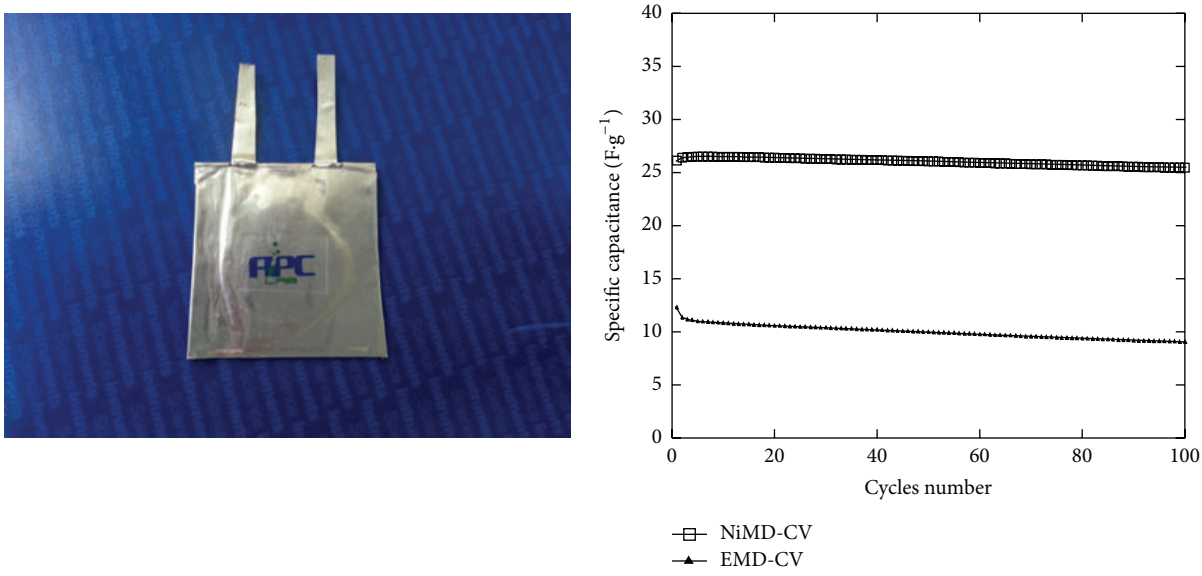

FIGURE 14: The prototype (left) and the charge-discharge test at 1 A·g^{-1} using thin film electrode of NiMD-CV and EMD-CV2 (right).

4. Conclusions

Nanoflakes EMD and NiMD with high porosity were prepared by two electrochemical depositions modes. The thin films exhibited the γ-MnO_2 based structure. The Ni addition to MnO_2 lattice affected the local structure of γ-MnO_2 that was evidently observed by using Raman spectroscopy. The EMD-CV exhibited better electrochemical behavior (C_{sp} and charge-discharge stability) than EMD-C due to the homogenous film forming and high porosity during the reduction-oxidation sweep. With short-time deposition (2 minutes), EMD thin films show the highest C_{sp} and lowest charge transfer resistance. Compared to EMD electrodes prepared at the same deposition, NiMD films enhance significantly the C_{sp} values as well as electrochemical stability. The highest C_{sp} value was 500 F·g^{-1} compared to 300 F·g^{-1} of EMD. The enhanced electrectrochemical performance of NiMD can be explained by the increase of thin film conductivity with the presence of ion Ni^{2+}. Moreover, high power density and excellent stability of assembled supercapacitor based on NiMD electrode materials were demonstrated (C_{sp} of 25 F·g^{-1} at 1 A·g^{-1}, 14% capacitance fade for 10,000 cycles).

Conflict of Interests

The authors declare that there is no conflict of interests regarding the publication of this paper.

Acknowledgments

The authors acknowledge funding from VNU-HCM under Grant HS2013-76-01. The authors would like to thank Office of Naval Research Global (ONRG) for Grant N62909-13-1-N235. The authors would like to thank the technical support of Horiba's Representative Company in Vietnam.

References

[1] H. Xia, M. O. Lai, and L. Lu, "Nanostructured manganese oxide thin films as electrode material for supercapacitors," *JOM*, vol. 63, no. 1, pp. 54–59, 2011.

[2] X. Zhao, B. M. Sánchez, P. J. Dobson, and P. S. Grant, "The role of nanomaterials in redox-based supercapacitors for next generation energy storage devices," *Nanoscale*, vol. 3, no. 3, pp. 839–855, 2011.

[3] W. Wei, X. Cui, W. Chen, and D. G. Ivey, "Manganese oxide-based materials as electrochemical supercapacitor electrodes," *Chemical Society Reviews*, vol. 40, no. 3, pp. 1697–1721, 2011.

[4] J. E. Post, "Manganese oxide minerals: crystal structures and economic and environmental significance," *Proceedings of the National Academy of Sciences of the United States of America*, vol. 96, no. 7, pp. 3447–3454, 1999.

[5] S. C. Pang, M. A. Anderson, and T. W. Chapman, "Novel electrode materials for thin-film ultracapacitors: comparison of electrochemical properties of sol-gel-derived and electrodeposited manganese dioxide," *Journal of the Electrochemical Society*, vol. 147, no. 2, pp. 444–450, 2000.

[6] S. C. Pang and M. A. Anderson, "Novel electrode materials for electrochemical capacitors. Part II. Material characterization of sol-gel-derived and electrodeposited manganese dioxide thin films," *Journal of Materials Research*, vol. 15, no. 10, pp. 2096–2106, 2000.

[7] N. Nagarajan, H. Humadi, and I. Zhitomirsky, "Cathodic electrodeposition of MnO_x films for electrochemical supercapacitors," *Electrochimica Acta*, vol. 51, no. 15, pp. 3039–3045, 2006.

[8] S. Hassa, M. Suzuki, and A. Abd El-Moneim, "Capacitive behavior of manganese dioxide/stainless steel electrodes at different deposition currents," *American Journal of Materials Science*, vol. 2, no. 2, pp. 11–14, 2012.

[9] C. Xu, B. Li, H. Du, F. Kang, and Y. Zeng, "Electrochemical properties of nanosized hydrous manganese dioxide synthesized by a self-reacting microemulsion method," *Journal of Power Sources*, vol. 180, no. 1, pp. 664–670, 2008.

[10] X. Hu, X. Lin, Z. Ling, Y. Li, and X. Fu, "Fabrication and characteristics of galvanostatic electrodeposited MnO_2 on porous nickel from etched aluminium," *Electrochimica Acta*, vol. 138, pp. 132–138, 2014.

[11] S. Hassan, M. Suzuki, and A. A. El-Moneim, "Effect of Ag-doping on the capacitive behavior of amorphous manganese dioxide electrodes," *Electrical and Electronic Engineering*, vol. 2, no. 2, pp. 18–22, 2012.

[12] T. Shinomiya, V. Gupta, and N. Miura, "Effects of electrochemical-deposition method and microstructure on the capacitive characteristics of nano-sized manganese oxide," *Electrochimica Acta*, vol. 51, no. 21, pp. 4412–4419, 2006.

[13] M. Minakshi, P. Singh, T. B. Issa, S. Thurgate, and R. De Marco, "Lithium insertion into manganese dioxide electrode in MnO_2/Zn aqueous battery Part II. Comparison of the behavior of EMD and battery grade MnO_2 in Zn—MnO_2— aqueous LiOH electrolyte," *Journal of Power Sources*, vol. 138, no. 1-2, pp. 319–322, 2004.

[14] T. Yousefi, R. Davarkhah, A. N. Golikand, and M. H. Mashhadizadeh, "Synthesis, characterization, and supercapacitor studies of manganese (IV) oxide nanowires," *Materials Science in Semiconductor Processing*, vol. 16, no. 3, pp. 868–876, 2013.

[15] J. Li and I. Zhitomirsky, "Cathodic electrophoretic deposition of manganese dioxide films," *Colloids and Surfaces A: Physicochemical and Engineering Aspects*, vol. 348, no. 1–3, pp. 248–253, 2009.

[16] J. Wei, M. Cheong, N. Nagarajan, and I. Zhitomirsky, "Cathodic electrodeposition of manganese oxides for electrochemical supercapacitors," *ECS Transactions*, vol. 3, no. 37, pp. 1–9, 2007.

[17] V. Subramanian, H. Zhu, R. Vajtai, P. M. Ajayan, and B. Wei, "Hydrothermal synthesis and pseudocapacitance properties of MnO_2 nanostructures," *The Journal of Physical Chemistry B*, vol. 109, no. 43, pp. 20207–20214, 2005.

[18] C. Ye, Z. M. Lin, and S. Z. Hui, "Electrochemical and capacitance properties of rod-shaped MnO_2 for supercapacitor," *Journal of the Electrochemical Society*, vol. 152, no. 6, pp. A1272–A1278, 2005.

[19] Q. T. Qu, P. Zhang, B. Wang et al., "Electrochemical performance of MnO_2 nanorods in neutral aqueous electrolytes as a cathode for asymmetric supercapacitors," *The Journal of Physical Chemistry C*, vol. 113, no. 31, pp. 14020–14027, 2009.

[20] J. P. Ni, W. C. Lu, L. M. Zhang, B. H. Yue, X. F. Shang, and Y. Lv, "Low-temperature synthesis of monodisperse 3D manganese oxide nanoflowers and their pseudocapacitance properties," *The Journal of Physical Chemistry C*, vol. 113, no. 1, pp. 54–60, 2009.

[21] X. Wang, A. Yuan, and Y. Wang, "Supercapacitive behaviors and their temperature dependence of sol-gel synthesized nanostructured manganese dioxide in lithium hydroxide electrolyte," *Journal of Power Sources*, vol. 172, no. 2, pp. 1007–1011, 2007.

[22] C. Julien, M. Massot, S. Rangan, M. Lemal, and D. Guyomard, "Study of structural defects in γ-MnO_2 by Raman spectroscopy," *Journal of Raman Spectroscopy*, vol. 33, no. 4, pp. 223–228, 2002.

[23] K. Rajendra Prasad and N. Miura, "Electrochemically synthesized MnO_2-based mixed oxides for high performance redox supercapacitors," *Electrochemistry Communications*, vol. 6, no. 10, pp. 1004–1008, 2004.